VIP Energy Storage Very Important Paper

Deutsche Ausgabe: DOI: 10.1002/ange.201603601
Internationale Ausgabe: DOI: 10.1002/anie.201603601

Perovskite $SrCo_{0.9}Nb_{0.1}O_{3-\delta}$ as an Anion-Intercalated Electrode Material for Supercapacitors with Ultrahigh Volumetric Energy Density

Liang Zhu, Yu Liu, Chao Su, Wei Zhou, Meilin Liu, and Zongping Shao**

Abstract: *We have synthesized and characterized perovskite-type $SrCo_{0.9}Nb_{0.1}O_{3-\delta}$ (SCN) as a novel anion-intercalated electrode material for supercapacitors in an aqueous KOH electrolyte, demonstrating a very high volumetric capacitance of about 2034.6 $F cm^{-3}$ (and gravimetric capacitance of ca. 773.6 $F g^{-1}$) at a current density of 0.5 $A g^{-1}$ while maintaining excellent cycling stability with a capacity retention of 95.7% after 3000 cycles. When coupled with an activated carbon (AC) electrode, the SCN/AC asymmetric supercapacitor delivered a specific energy density as high as 37.6 $Wh kg^{-1}$ with robust long-term stability.*

As an important means of electrical energy storage through electrical double layer capacitance or pseudocapacitance, supercapacitors have received tremendous attention during the past decade.[1] The unique performance characteristics of supercapacitors, such as high power density and long cycling life, make them ideally suited to bridging the energy/power gaps between conventional dielectric capacitors and batteries.[2] When supercapacitors are used as the main or auxiliary power source for electric vehicles and portable electronics, high volumetric energy density is essential due to limited space besides long life and high gravimetric energy density. Supercapacitors with carbon-based electrodes or electrical double layer capacitors (EDLCs) usually have low volumetric energy density because of the low tap density of high-surface-area carbon materials. In contrast, pseudocapacitors store energy via redox reactions at the surface or subsurface of the electrodes, demonstrating much higher specific capacitance than carbon-based EDLCs.[3] However, a high specific surface area is also required to achieve high capacitance, which is unfavorable for volumetric energy density due to low tap density of the electrodes.

Recently, supercapacitors that store energy through ion intercalation into electrode bulk, similar to lithium-ion batteries, have attracted much attention.[4] Because of the bulk intercalation mechanism, high surface area is no longer required to ensure high capacity. To date, most of the intercalation-type supercapacitor electrodes are based on positive ion as the charge carrier,[4b,d,5] while anions are considered less favorable because of their large ion size. Recently, Mefford et al. demonstrated that the oxygen ion can also be effectively used as a charge carrier to realize a new type of anion-intercalated supercapacitors, and reported gravimetric capacitance of about 609.8 $F g^{-1}$ for $LaMnO_{3-\delta}$ perovskite in an aqueous KOH electrolyte.[4e] Cao et al. also reported the capacitor performance of Sr-doped $LaCoO_3$ and Sr-doped $LaNiO_3$ perovskites.[6]

Since oxygen vacancies are the charge carriers, increasing oxygen vacancy concentration may enhance the capacitance of the oxygen-ion-intercalation electrodes. To realize the incorporation of oxygen-ion into oxygen vacancies, it requires the simultaneous oxidation state change of the cations in the oxide electrodes; thus the oxides should have good redox capability. Additionally, high oxygen vacancy mobility is crucial to achieving high power density in order to facilitate fast oxygen-anion intercalation during charge storage. Cobalt-based perovskites are superior to Mn-based ones due to their larger oxygen vacancy concentration and higher oxygen-ion mobility.[7]

Here we report our findings in synthesis and characterization of $SrCo_{0.9}Nb_{0.1}O_{3-\delta}$ (SCN) perovskite as an outstanding electrode material for supercapacitors in an aqueous KOH electrolyte at room temperature; SCN is a mixed ionic-electronic conductor that shows superior performance as a cathode for solid oxide fuel cells and as an oxygen-separation-membrane due to its fast surface oxygen exchange kinetics, excellent oxygen mobility, and large oxygen vacancy concentration at elevated temperatures.[8] High tap-density SCN was synthesized by a facile solid-state reaction. When tested in a supercapacitor, the anion-intercalated SCN electrode showed high capacitance, excellent rate capability, and favorable cycling stability. Furthermore, when coupled with an AC electrode, the SCN/AC asymmetric supercapacitor (ASC) delivered superb energy density, outperforming

[*] L. Zhu, Prof. W. Zhou
State Key Laboratory of Materials-Oriented Chemical Engineering
College of Chemistry & Chemical Engineering
Jiangsu National Synergetic Innovation Center for Advanced Materials (SICAM), Nanjing Tech University
No. 5 Xin Mofan Road, Nanjing 210009 (P.R. China)
Y. Liu, Dr. C. Su, Prof. Z. P. Shao
Department of Chemical Engineering, Curtin University
Perth, Western Australia 6845 (Australia)
Prof. L. M. Liu
Center for Innovative Fuel Cell and Battery Technologies
School of Materials Science and Engineering
Georgia Institute of Technology
Atlanta, GA 30332-0245 (USA)
E-mail: meilin.liu@mse.gatech.edu
Prof. Z. P. Shao
State Key Laboratory of Materials-Oriented Chemical Engineering, College of Energy, Jiangsu National Synergetic Innovation Center for Advanced Materials (SICAM), Nanjing Tech University
No. 5 Xin Mofan Road, Nanjing 210009 (P.R. China)
E-mail: shaozp@njtech.edu.cn

Supporting information for this article can be found under: http://dx.doi.org/10.1002/anie.201603601.

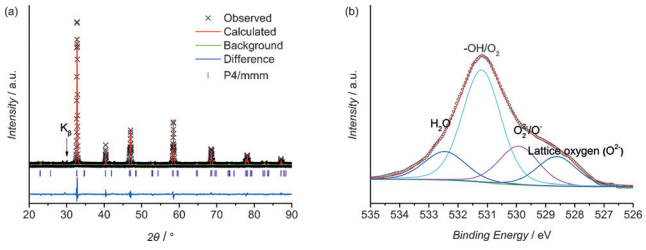

Figure 1. a) Refined XRD patterns of the fresh SCN. b) XPS spectrum of O1s in the fresh SCN. The arrows indicate weak peaks representing the (110) plane of SCN at ≈29.6° (2θ) because of the high intensity of the X-ray beam (K_β = 1.3923 Å).

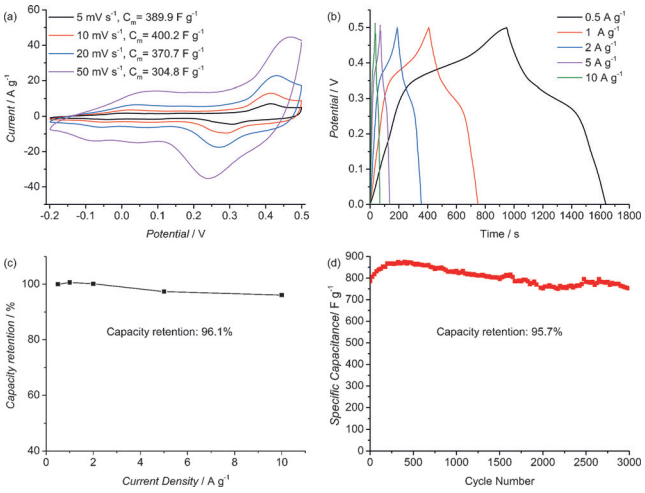

Figure 2. a) CV curves of SCN electrode at various scan rates. b) GCD curves and c) capacity retention of SCN at various current densities. d) Specific capacitance of SCN as a function of cycle numbers.

most of reported ASCs, suggesting that SCN has potential to be a promising electrode material for next-generation supercapacitors for a wide range of applications.

The Rietveld refinement of SCN XRD pattern (Figure 1a) revealed a tetragonal structure with lattice parameters of $a = 3.8070(0)$ Å and $c = 7.776(0)$ Å and a space group of P4/mmm. After treating in Ar (SCN^A) or 10% H_2/Ar (SCN^H) atmosphere, SCN still maintained the tetragonal structure without any second phases (see Figure S1 in the Supporting Information). A small change in lattice parameters was observed as large amount of oxygen was extracted from the SCN lattice (Table S1), which is beneficial for a stable cycling performance as an anion-intercalated electrode for supercapacitor. The amount of oxygen vacancies were 10.3, 10.6, and 19.4% of oxygen sites in SCN, SCN^A and SCN^H, respectively (Table S2), suggesting 9.1% of oxygen in SCN lattice can be used for energy storage, corresponding to a capacitance of 546 $F g^{-1}$. The as-prepared SCN showed irregular grain shape, large grain size of ≈1 μm, pore-free nature, and low Brunauer-Emmett-Teller (BET) specific surface area of ≈8.63 $m^2 g^{-1}$ (Figures S2 & S3). The tap density of the obtained SCN is 2.63 $g cm^{-3}$, resulting in high volumetric energy density of the electrode. The O1s XPS spectrum of SCN, SCN^A and SCN^H (Figure 1b, Figure S4 & Table S3) can be deconvoluted into four characteristic peaks: lattice oxygen species (O^{2-}) at 528.7 eV, highly oxidative oxygen species (O_2^{2-}/O^-) at 530.0 eV, hydroxy groups (−OH) or surface-adsorbed O_2 at 531.0 eV, and surface-adsorbed H_2O at 532.0 eV.[9] The amount of O_{ads} species is intimately associated with the oxygen vacancy density of perovskite oxide.[10]

Because of the similar electrochemical performance of the SCN samples with different amount of oxygen vacancies, here we present the electrochemical performance of the fresh SCN (Figure S5). The electrochemical performance of the fresh SCN electrode was evaluated using cyclic voltammetry (CV) in KNO_3 (Figure S6) and KOH electrolytes, respectively. The specific capacitance of the SCN electrode increased to 400.2 $F g^{-1}$ at 10 $mV s^{-1}$ in the KOH electrolyte, which was 30-fold higher than that in the KNO_3 solution (Figure 2a). It suggests the intercalation-type energy storage was likely appeared with the presence of OH^-. All the CV curves exhibited two pairs of redox peaks related to Co^{2+}/Co^{3+} and Co^{3+}/Co^{4+}, indicating the capacitance of SCN were mainly governed by faradic redox reactions. Additionally, the peak current increased with the scan rate, suggesting electronic- and ionic-transport rates were sufficiently rapid.[11] Note that the background signal due to the Ni foam was negligible (Figure S7). The Galvanostatic charge–discharge (GCD) curves of the SCN electrode (Figure 2b) displayed a typical pseudocapacitance behavior, demonstrating higher gravimetric, areal, and volumetric capacitances (C_m, C_a, and C_v) at different current densities (Table S4) than those of most state-of-the-art materials (e.g. carbon, RuO_2).[12] Such ultrahigh specific capacitance provided a strong support for the participation of SCN bulk phase in the energy storage. Because no phase transition happened during the O^{2-} intercalation or extraction process (Figure S8), the GCD curves did not show the platform that was typical for a two-phase electrode reaction process. Instead, the shapes of the curves reflect a typical supercapacitor behavior.[4a] The outstanding rate capability (based on the GCD curves), indicated by a slight decrease (ca. 3.9%) in the capacitance as the current density was increased from 0.5 to 10 $A g^{-1}$ (Figure 2c), implies rapid surface reaction and O^{2-} bulk diffusion, which was supported by a low charge transfer resistance of the electrode (0.1111 Ω) and a high oxygen diffusion rate (1.1×10^{-12} $cm^2 s^{-1}$; Figures S9 and S10). The cycling stability is a big concern because large volume change may occur during the process that could pulverize the electrode and deteriorate electrode activity. As shown in Figure 2d, the initial specific capacitance was ≈786.1 $F g^{-1}$, and progressively increased in the first 250 cycles, followed by a slow decrease in the subsequent cycles. Nevertheless, ≈752.6 $F g^{-1}$ was still retained after 3,000 cycles, indicating excellent cycling stability.

Based on above analysis and literatures,[4e,8a] the charge storage mechanism of the SCN electrode can be expressed as shown in Equation (1) and (2).

$$Sr[Co^{2+}_{2\delta}; Co^{3+}_{(0.9-2\delta)}]Nb^{5+}_{0.1}O_{2.6-\delta} + 2\delta OH^- \rightleftharpoons SrCo^{3+}_{0.9}Nb^{5+}_{0.1}O_{2.6} + 2\delta e^- + \delta H_2O \quad (1)$$

$$SrCo^{3+}_{0.9}Nb^{5+}_{0.1}O_{2.6} + 2\delta OH^- \rightleftharpoons Sr[Co^{4+}_{2\delta}; Co^{3+}_{(0.9-2\delta)}]Nb^{5+}_{0.1}O_{2.6+\delta} + 2\delta e^- + \delta H_2O \quad (2)$$

Oxygen vacancies were filled through intercalation of an electrolyte oxygen ion via OH^- and diffusion of O^{2-} along the edges of unit cell; meanwhile, Co^{2+} was oxidized to Co^{3+}. Excess O^{2-} was intercalated on the surface by the Co^{3+} diffusion and oxidation. The surface reaction for the incorporation of O^{2-} from OH^- into oxygen vacancies was more complicated in real case, which may involve several steps with the formation of various intermediate O_{ads} species as supported by the XPS (Figure 1b). Further understanding of the charge storage mechanism may be obtained through in situ/operando synchrotron-enabled X-ray analyses.[13]

In the anion-intercalated supercapacitor, the OH^- adsorption over the electrode surface (capacitive process) and O^{2-} diffusion within the oxide bulk are involved. The peak current (i) of CV curve and sweep rate (ν) typically obey the power-law relationship ($i = a\nu^b$).[14] As shown in Figure 3a, b values

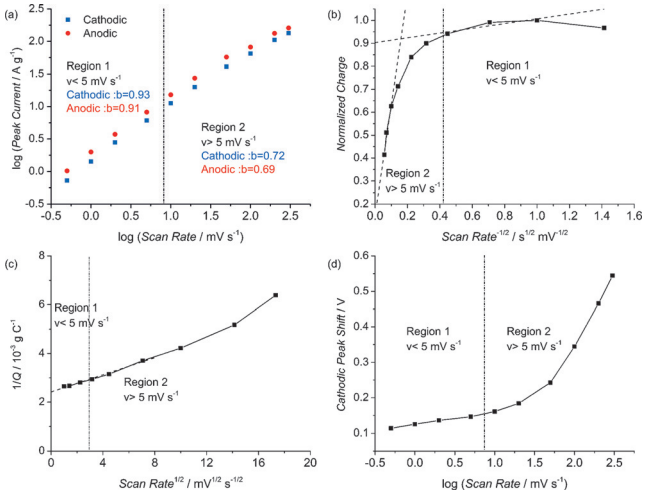

Figure 3. a) The b value determination of normalized anodic and cathodic peak currents. b) Plot of Q versus $\nu^{-1/2}$. c) Plot of Q^{-1} versus $\nu^{1/2}$. d) Profile of the cathodic peak shift of SCN.

of both cathodic and anodic peaks are close to 1 at region 1 ($\nu < 5\,mV\,s^{-1}$), indicating the capacitive process. At region 2 ($\nu > 5\,mV\,s^{-1}$), b values are close to 0.5 for both peaks, suggesting the O^{2-} diffusion is the rate-limiting step.[15] The relationship between capacity (normalized charge, Q) and ν can also establish the rate-limiting step.[16] In region 1 of Figure 3b, the charge was not sensitive to the variation of scan rate, which means charge storage is not controlled by diffusion. Moreover, the extrapolated y-intercept yields the capacitance of $303.0\,C\,g^{-1}$ at the infinite sweep rate.[4b] In region 2, the capacity near linearly decreased with increasing scan rates, implying the O^{2-} diffusion controls the charge storage. The capacitance associated with the specific surface area, estimated by extrapolation of the plot in region 2, is only $56.4\,C\,g^{-1}$, which is a quite small portion in the entire capacitance. Therefore, the high capacitance is mainly contributed from the high rate insertion of O^{2-}. For further confirmation this implication, the capacitance at the infinite sweep rate was also obtained by extrapolating the plot of Q^{-1} vs. $\nu^{-1/2}$ in region 1 (Figure 3c). The result is $381.5\,C\,g^{-1}$, which is close to $303.0\,C\,g^{-1}$. As shown in Figure 3d, another feature of the capacitive behavior at region 1 was the relatively small peak-potential-shift (< 0.15 V). It is a good indication of the facile insertion of O^{2-} because the slow diffusion-controlled process will result in much larger peak shifts such as in LIBs.[4b]

To demonstrate the feasibility of SCN in practical energy storage devices, an asymmetric supercapacitor (ASC) was assembled using SCN and AC as the cathode and anode, respectively. The stable electrochemical potential window of the SCN/AC ASC can be extended to 1.5 V (Figure S11). CV curves of the ASC at various scan rates demonstrated its excellent capacitive behavior (Figure 4a). 86.1% of the

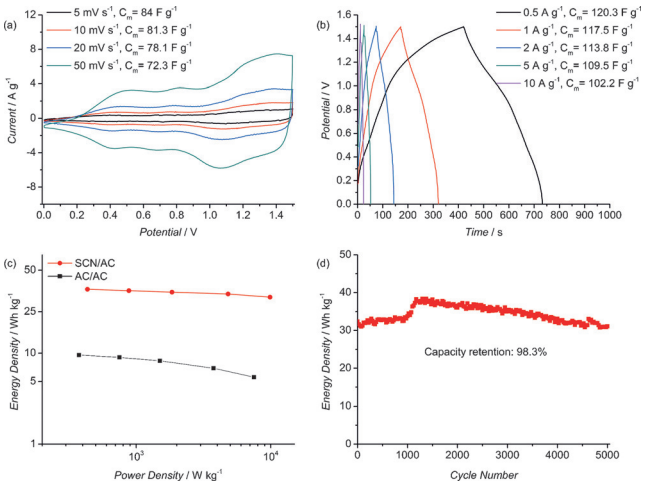

Figure 4. a) CV curves at various scan rates and b) GCD curves at various current densities of the SCN/AC ASC. c) Ragone plots of the SCN/AC and AC/AC supercapacitors. d) Cycling stability of SCN/AC ASC.

specific capacitance was retained when the scan rate was increased from 5 to $50\,mV\,s^{-1}$. The specific capacitance calculated from GCD curves also showed a similar trend (Figure 4b). Ragone plots (Figure 4c) show that an energy density of $37.6\,Wh\,kg^{-1}$ was achieved at an average power density of $433.9\,W\,kg^{-1}$ for the ASC. Even at a high power density of $9864.2\,W\,kg^{-1}$, the energy density of $32.9\,Wh\,kg^{-1}$ was retained, approaching the lower end of lithium ion batteries.[17] Our ASC delivered much higher performance than many reported results (Table S5). As shown in Figure 4d, the specific energy decreased by only $\approx 1.7\%$ after 5,000 cycles, suggesting robust stability and long operational life.

In summary, the tetragonal SCN with high oxygen-vacancy concentration was developed as an electrode material for supercapacitors, demonstrating high volumetric and gravimetric capacitance and stable cycling performance. The SCN/AC asymmetric supercapacitor displayed high specific energy and outstanding stability. It is also shown that the perovskite materials can achieve high capacitance through the anion-insertion mechanism, paving a new way for the

development of supercapacitors with high energy and power density. The SCN has potential as a remarkable electrode in the next-generation high-performance supercapacitors.

Acknowledgements

This work was supported by the Changjiang Scholars Program under contract number T2011170, the "Key Projects in Nature Science Foundation of Jiangsu Province" under contract number BK2011030, the "Major Project of Educational Commission of Jiangsu Province of China" under contract number 13KJA430004, the Project of Priority Academic Program Development of Jiangsu Higher Education Institutions and the Chinese Academy of Sciences Innovative and Interdisciplinary Team Award.

Keywords: electrodes · energy storage · oxygen vacancy · perovskite oxides · supercapacitors

How to cite: *Angew. Chem. Int. Ed.* **2016**, *55*, 9576–9579
Angew. Chem. **2016**, *128*, 9728–9731

[1] a) R. F. Service, *Science* **2006**, *313*, 902–902; b) J. R. Miller, P. Simon, *Science* **2008**, *321*, 651–652; c) D. Liu, B. B. Garcia, Q. Zhang, Q. Guo, Y. Zhang, S. Sepehri, G. Cao, *Adv. Funct. Mater.* **2009**, *19*, 1015–1023.

[2] a) X. Chen, B. Zhao, Y. Cai, M. O. Tade, Z. Shao, *Nanoscale* **2013**, *5*, 12589–12597; b) B. E. Conway, *J. Electrochem. Soc.* **1991**, *138*, 1539–1548; c) P. Simon, Y. Gogotsi, *Nat. Mater.* **2008**, *7*, 845–854.

[3] a) C. Guan, X. Li, Z. Wang, X. Cao, C. Soci, H. Zhang, H. J. Fan, *Adv. Mater.* **2012**, *24*, 4186–4190; b) T. Y. Wei, C. H. Chen, H. C. Chien, S. Y. Lu, C. C. Hu, *Adv. Mater.* **2010**, *22*, 347–351; c) M. Xue, Z. Xie, L. Zhang, X. Ma, X. Wu, Y. Guo, W. Song, Z. Li, T. Cao, *Nanoscale* **2011**, *3*, 2703–2708.

[4] a) M. Zhu, W. Meng, Y. Huang, Y. Huang, C. Zhi, *ACS Appl. Mater. Interfaces* **2014**, *6*, 18901–18910; b) V. Augustyn, J. Come, M. A. Lowe, J. W. Kim, P. L. Taberna, S. H. Tolbert, H. D. Abruña, P. Simon, B. Dunn, *Nat. Mater.* **2013**, *12*, 518–522; c) M. R. Lukatskaya, O. Mashtalir, C. E. Ren, Y. Dall'Agnese, P. Rozier, P. L. Taberna, M. Naguib, P. Simon, M. W. Barsoum, Y. Gogotsi, *Science* **2013**, *341*, 1502–1505; d) T. Brezesinski, J. Wang, S. H. Tolbert, B. Dunn, *Nat. Mater.* **2010**, *9*, 146–151; e) J. T. Mefford, W. G. Hardin, S. Dai, K. P. Johnston, K. J. Stevenson, *Nat. Mater.* **2014**, *13*, 726–732.

[5] T. Brezesinski, J. Wang, J. Polleux, B. Dunn, S. H. Tolbert, *J. Am. Chem. Soc.* **2009**, *131*, 1802–1809.

[6] a) Y. Cao, B. Lin, Y. Sun, H. Yang, X. Zhang, *Electrochim. Acta* **2015**, *178*, 398–406; b) Y. Cao, B. Lin, Y. Sun, H. Yang, X. Zhang, *Electrochim. Acta* **2015**, *174*, 41–50.

[7] a) Z. Zhang, W. Zhou, Y. Chen, D. Chen, J. Chen, S. Liu, W. Jin, Z. Shao, *ACS Appl. Mater. Interfaces* **2015**, *7*, 22918–22926; b) G. Kim, S. Wang, A. Jacobson, L. Reimus, P. Brodersen, C. Mims, *J. Mater. Chem.* **2007**, *17*, 2500–2505.

[8] a) K. Zhang, R. Ran, L. Ge, Z. Shao, W. Jin, N. Xu, *J. Membr. Sci.* **2008**, *323*, 436–443; b) F. Wang, Q. Zhou, T. He, G. Li, H. Ding, *J. Power Sources* **2010**, *195*, 3772–3778.

[9] Y. Wang, J. Ren, Y. Wang, F. Zhang, X. Liu, Y. Guo, G. Lu, *J. Phys. Chem. C* **2008**, *112*, 15293–15298.

[10] a) Y. M. Yin, M. W. Xiong, N. T. Yang, Z. Tong, Y. Q. Guo, Z. F. Ma, E. Sun, J. Yamanis, B. Y. Jing, *Int. J. Hydrogen Energy* **2011**, *36*, 3989–3996; b) J. Hu, L. Wang, L. Shi, H. Huang, *J. Power Sources* **2014**, *269*, 144–151.

[11] D. Guo, H. Zhang, X. Yu, M. Zhang, P. Zhang, Q. Li, T. Wang, *J. Mater. Chem. A* **2013**, *1*, 7247–7254.

[12] a) J. P. Randin, E. Yeager, *J. Electrochem. Soc.* **1971**, *118*, 711–714; b) X. Wu, Y. Zeng, H. Gao, J. Su, J. Liu, Z. Zhu, *J. Mater. Chem. A* **2013**, *1*, 469–472.

[13] M. Salanne, B. Rotenberg, K. Naoi, K. Kaneko, P.-L. Taberna, C. Grey, B. Dunn, P. Simon, *Nat. Energy* **2016**, *1*, 16070.

[14] H. Lindström, S. Södergren, A. Solbrand, H. Rensmo, J. Hjelm, A. Hagfeldt, S. E. Lindquist, *J. Phys. Chem. B* **1997**, *101*, 7717–7722.

[15] M. Park, X. Zhang, M. Chung, G. B. Less, A. M. Sastry, *J. Power Sources* **2010**, *195*, 7904–7929.

[16] S. Ardizzone, G. Fregonara, S. Trasatti, *Electrochim. Acta* **1990**, *35*, 263–267.

[17] X. Yu, B. Lu, Z. Xu, *Adv. Mater.* **2014**, *26*, 1044–1051.

Received: April 13, 2016
Published online: July 1, 2016

